Lattice dynamics of layered-structure compounds: $PdTe_2$

T. R. Finlayson,* W. Reichardt,† and H. G. Smith
Solid State Division, Oak Ridge National Laboratory, Oak Ridge, Tennessee 37830
(Received 26 February 1985)

A complete data set for the phonon dispersion curves of $PdTe_2$ along the [ζ00], [ζζ0], and [00ζ] symmetry directions has been measured. A lattice-dynamical model consisting of axially symmetric Born—von Kármán interactions to seventh-nearest neighbors together with shell-model contributions, introduced specifically to model dips in the low-energy optic branches in the vicinity of the Γ point, provides a reasonable fit to the measured dispersion curves. The results are discussed in relation to the known properties of $PdTe_2$ and the dispersion data already available for related layered-structure compounds.

I. INTRODUCTION

$PdTe_2$, with the CdI_2 structure [space group D_{3d}^3 ($P\bar{3}m$ 1)], has been classified amongst the superconducting transition-metal dichalcogenides (TMDC's).[1] The superconducting transition temperature (T_c) for $PdTe_2$ is only 1.7 K, but this compares favorably with the transition temperatures for other TMDC's.[2] These compounds, of general formula MX_2, consist of a group-IV to -VIII metal M and a chalcogen atom X (S, Se, or Te) and they crystallize in various polytypes composed of X-M-X sandwiches. In general, for the superconducting members, the M-X coordination is trigonal prismatic (TP). $PdTe_2$ is the notable exception to this generalization since for it the M-X coordination is octahedral (O). Most of the other O coordination TMDC's show semiconducting or semimetallic properties.[1]

The structure, illustrated in Fig. 1, is best described on a hexagonal basis with one palladium and two tellurium atoms per unit cell having lattice parameters $a=4.0365$ Å and $c=5.1262$ Å. The resultant c/a ($=1.27$) is the smallest value amongst the isoelectronic, isostructural TMDC's. (For $PtTe_2$ and $NiTe_2$ c/a is 1.297 and 1.368, respectively.) All other CdI_2 structure TMDC's show c/a close to the ideal value of 1.633 for this structure while for the other superconducting TMDC's c/a is close to or even greater than the ideal value for their structures.[1] Thus, discussion of the superconductivity of the TMDC's has emphasized the highly anisotropic, partly two-dimensional character of these compounds,[3] an aspect which is further exemplified by the occurrence of superconductivity amongst some intercalated TMDC's.[2]

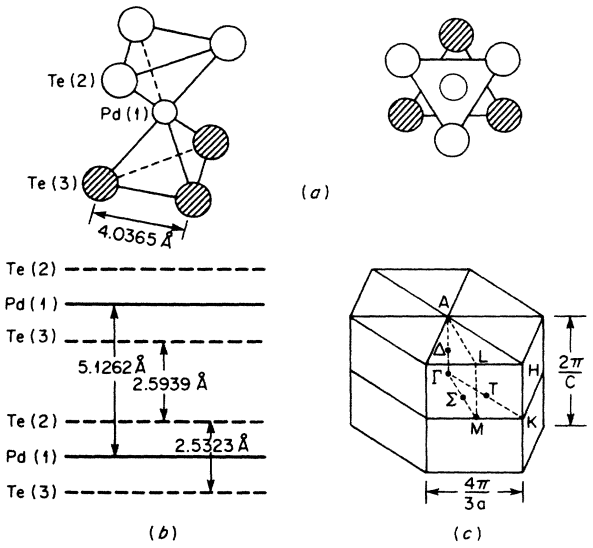

FIG. 1. Crystal structure for $PdTe_2$ showing (a) octahedral coordination within each sandwich, (b) the stacking of the sandwiches, and (c) the hexagonal Brillouin zone.

The observation of charge-density-wave (CDW) transitions in some TMDC's has also been a point of discussion in relation to their superconductivity. For example, in the series $TaS_{2-x}Se_x$ the addition of the alloying element to either of the pure end members leads to an enhancement of T_c but a suppression of the CDW transition.[4] Also the application of pressure gives rise to an enhancement of T_c and a suppression of the CDW transition.[5] The CDW results from a lowering of the crystal free energy by the appearance of a gap at the Fermi level at a particular wave vector q, at which anomalous phonon dispersion at 300 K and marked phonon softening on reduction of temperature below 300 K have been observed.[6] For the superconducting compounds $2H$-$TaSe_2$ and $2H$-$NbSe_2$ q is close to $(\frac{1}{3},0,0)$ and thus the phonon anomalies are found in the [ζ00] branch near this wave vector. However, CDW transitions are not confined to the superconducting TMDC's. In the semimetal, $1T$-$TiSe_2$, for example, a CDW transition leading to the appearance of superlattice reflections at $\mathbf{q}=(\frac{1}{2},0,\frac{1}{2})$ has been demonstrated by electron and x-ray diffraction.[7] A soft phonon of wave vector $(\frac{1}{2},0,\frac{1}{2})$ with purely transverse polarization has been associated with this transition.[8,9] These observations together with the results of a simple force-constant model for the existing phonon dispersion data[9] indicate that $1T$-$TiSe_2$ exhibits more three-dimensional character than the superconducting materials.

On account of the similarity in crystal structures between $1T$-$TiSe_2$ and $PdTe_2$, it is tempting to compare the

lattice dynamics for these two compounds. However, there are no reports of structural anomalies in $PdTe_2$. The temperature dependence of the Hall coefficient, measured with the applied field perpendicular to the basal (cleavage) plane was studied from 4.2 to 300 K.[10] The Hall coefficient was positive over the entire temperature range with a value of 3.3×10^{-16} m^3/C at 4.2 K and decreased steadily to 2.2×10^{-16} m^3/C with increasing temperature. No anomalous behavior indicative of a phase transition was found. A study of the pressure dependence of T_c (Ref. 10) showed a broad maximum of 2 K at a pressure of 0.5 GPa. This unusual behavior has been interpreted as arising from a variation in the electronic density of states at the Fermi level which, on the basis of a band-structure calculation,[11] lies in the vicinity of a local minimum on one of the Te-Pd hybridized energy bands.

Existing data for the phonon dispersion of most of the TMDC's suffer from the disadvantage that crystals have invariably been small, and thus there is no complete data set for these compounds. $PdTe_2$, on the other hand, crystallizes very readily and a roughly cylindrical sample, $\sim$60 mm long and $\sim$12 mm in diameter, grown and used for a previous purpose,[12] provided the initial stimulus for measuring the dispersion curves, in the hope of gaining some understanding of the superconductivity in this material.

In this paper we present the experimental data and model calculations using combinations of axially symmetric force constants and shell interactions and discuss the results in relation to the measured phonon dispersion data for related compounds and the known properties of $PdTe_2$.

II. EXPERIMENTAL DETAILS

The $PdTe_2$ crystal used in this investigation was prepared by the Bridgeman technique. The nominal amounts of spectrochemically pure palladium sponge and tellurium block of 99.999% purity were sealed into an evacuated silica tube (25 mm diam) and reacted together for 24 h at 850°C. The product was then crushed and sealed under vacuum into a 15-mm-diam pointed silica crucible. The Bridgeman furnace was set to have a hot zone at 800°C below which the temperature decreased at approximately 0.6°C/mm.[13] After keeping the sample in the hot zone for 5 h, it was lowered through the temperature gradient at 2.4 mm/h.

It was found necessary to cleave from the main crystal some material which appeared to have an orientation different from the rest. The resultant specimen for the neutron experiment was a 30-g crystal 60 mm long and 12 mm in diameter with a mirrorlike cleavage plane passing obliquely along its length. The neutron rocking curve of the crystal was slightly asymmetrical with a half-width of 0.5°. Crystallographic data for the crystal are given in Fig. 1. The superconducting transition temperature which was measured on a small piece of the crystal by the mutual inductance technique was found to be 1.5 K.

The room-temperature neutron inelastic scattering was carried out primarily on the HB-3 spectrometer at the High Flux Isotope Reactor at Oak Ridge National Laboratory using 40-min collimators before and after the specimen. The monochromator and analyzer were the Be(002) planes with the latter set for a fixed final energy of 8 THz. The data from this spectrometer were collected under conditions of energy loss by the incident neutrons. Some preliminary data for the [100]-[001] scattering plane were collected on the HB-1A spectrometer using the pyrolytic graphite (002) planes as both monochromator and analyzer, with a fixed incident energy of 3.57 THz and operating under energy gain conditions. Finally, some data were collected at 10 K, with the specimen mounted in a Displex closed-cycle helium refrigerator on the HB-2 spectrometer. In this case both the monochromator and the analyzer were the pyrolytic graphite (002) planes, collimation was 20 min before and after the specimen and the spectrometer was operated for energy loss with a fixed final energy of 8 THz. To collect the complete data set the crystal was mounted in three different orientations. Phonon scans were performed in the constant-Q mode except for the longitudinal acoustic branch in the $[\zeta\zeta0]$ direction for $q<0.15$ $(4\pi/a)$ which was measured in the constant-E mode.

III. RESULTS

The Brillouin zone and the usual labels for symmetry points and directions have been reproduced in Fig. 1. In Table I we have identified the symmetry characteristics for the lattice modes of the $PdTe_2$ structure at several points in the Brillouin zone.

The data for each of the symmetry directions $[\zeta00]$, $[\zeta\zeta0]$, and $[00\zeta]$ are reproduced in Fig. 2. The lines drawn through the experimental points are intended to be a guide to the eye. In general the phonon groups were separate and well defined. Measured values for the full width at half maximum from constant-Q scans ranged from 0.25 THz for some of the low-q transverse acoustic phonons to 0.8 THz for some of the optic modes. For the few constant-E scans undertaken for the $[\zeta\zeta0]$ longitudinal phonons, δq at half the maximum intensity for the measured peaks was of order 0.05 $(4\pi/a)$. The frequencies of equivalent phonons measured at different lattice points and on the different spectrometers used, were found to be in agreement to better than 0.1 THz which is typical of the largest experimental errors involved in determining peak frequencies from the various scans. Representative error bars are indicated in Fig. 2.

For the low-energy data in the $[\zeta\zeta0]$ directions with $q>0.25(4\pi/a)$ and to a lesser extent in the $[\zeta00]$ direction for $q>0.4(4\pi/a)$, assignment of frequencies and branches became extremely difficult due to overlap of acoustic and low-energy optic phonons. The assignments made on Fig. 2 have been accomplished with the aid of structure-factor calculations using a model for the lattice dynamics of $PdTe_2$ which will be described in the next section. With the knowledge of these structure factors, overlapping peaks in the raw data could be consistently resolved. The branches in Fig. 2 have been labeled according to the irreducible representations. Note in particular that the modes on the low-energy optic branches, Σ_1 and T_2 at low q, are almost purely longitudinal, but have

TABLE I. Irreducible representations and symmetry characteristics for lattice modes in $PdTe_2$ (Ref. 14).

Irreducible representation: Modified Koster notation	Mulliken notation	Atom vibration directions Pd=(1), Te=(2,3)	Displacements of Te atoms
Γ_1^+	A_g	(1) None; (2,3) z	equal and opposite
Γ_1^-	A_u	(1,2,3) z	equal
Γ_2^+	E_g	(1) none; (2,3) x or y	equal and opposite
Γ_2^-	E_u	(1,2,3) x or y	equal
T_1	A	(1) x; (2,3) x,y,z	equal along x
T_2	B	(1) y,z; (2,3) x,y,z	equal and opposite along y,z
M_1^+	A_g	(1) none: (2,3) y,z	equal and opposite
M_1^-	A_u	(1,2,3) x	equal
M_2^+	B_g	(1) none; (2,3) x	equal and opposite
M_2^-	B_u	(1,2,3) y,z	equal
Σ_1	A'	(1,2,3) y,z	
Σ_2	A''	(1,2,3) x	
Δ_1	A_1	(1,2,3) z	
Δ_2	E	(1,2,3) x or y	

the same irreducible representations as the lowest-energy transverse modes in the [ζ00] and [$\zeta\zeta$0] directions, respectively.

At the M point the frequencies of the M_1^+ and M_2^- modes near 2.5 THz and those of the M_1^- and M_2^- modes near 3 THz coincide, within the accuracy of our experiment. Thus, in Fig. 2 these pairs of frequencies have been marked by single points in each case. These coincidences are accidental and are not required by symmetry. The degeneracies at the K point indicated on the figure are expected from symmetry.

Other features of the results which are of particular in-

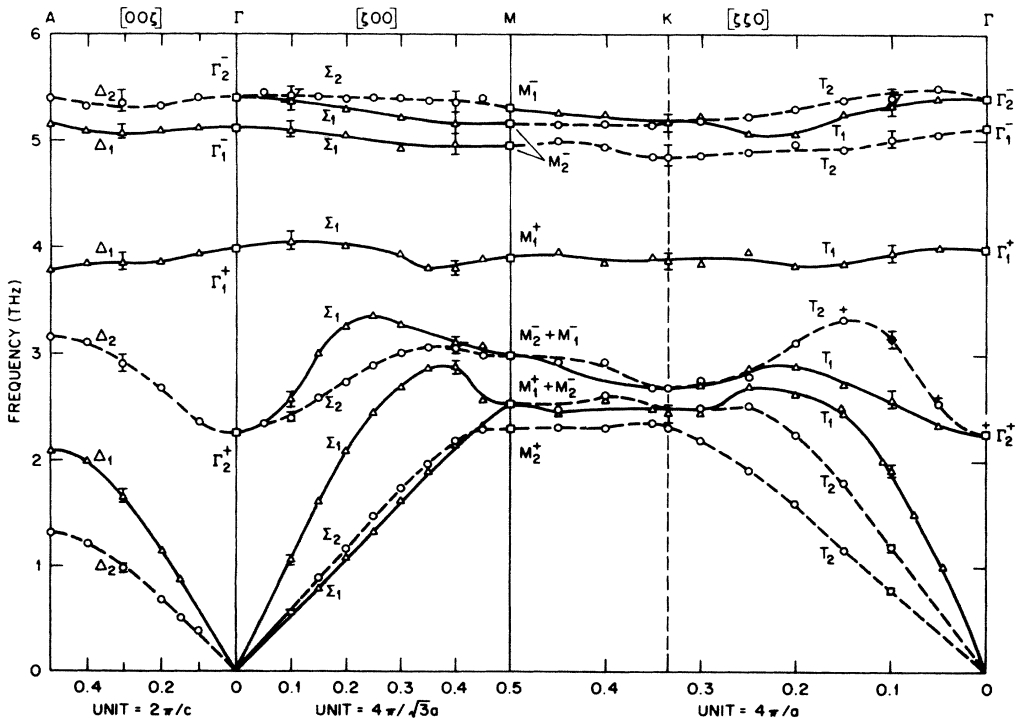

FIG. 2. Measured room-temperature phonon dispersion curves for the symmetry directions (ζ00), ($\zeta\zeta$0), and (00ζ) for $PdTe_2$. The lines drawn through the data are a guide to the eye. Four frequencies along the T_2 branch in the vicinity of the Γ_2^+ point were measured at 10 K and are indicated by the (+) symbol.

terest are the pronounced dips in some low-energy optic branches (Δ_2, Σ_1, T_2) in the vicinity of Γ_2^+. We want to emphasize that the structures observed in these branches are *not* caused by hybridization with other branches. This is quite obvious for the [$\zeta\zeta$0] direction as the T_2 branch and the T_1 branch around 4 THz belong to different irreducible representations. While in [ζ00] directions the corresponding branches have the same symmetry, their mutual interaction is small. However, there is a strong interaction between the upper Σ_1 branch and the longitudinal acoustic Σ_1 branch which results in an anticrossing behavior near $q=0.35(4\pi/\sqrt{3}a)$.

The Γ_2^+ frequency and a few T_2 phonons were also measured at 10 K in the hope of revealing some origin for this anomaly. The results are indicated by the four crosses in Fig. 2. A normal temperature dependence with a slight stiffening on cooling was observed.

IV. MODEL CALCULATION

The dispersion curves for $PdTe_2$ have been calculated using a generalized computer program which had been written for crystal structures with orthogonal lattice vectors. In order to apply this program to a hexagonal lattice we chose a base-centered orthogonal unit cell of dimensions $a\times b\times c=a_h\times\sqrt{3}a_h\times c_h$, where a_h and c_h are the lattice constants for the hexagonal unit cell. In order to ensure that the program treats reduced lattice vectors like (2,0,0) and (1,1,0) to be identical we had to restrict the lattice-dynamical model to one of axially symmetric forces.

It is apparent from the experimental data, and has been confirmed by the calculations, that the measured dispersion curves for $PdTe_2$ cannot be reproduced by a simple force-constant model with short-range interactions only. This is especially true for the dips in the low-frequency optic branches in the vicinity of the Γ point. Therefore, we included in the model shell interactions of the same kind as have been introduced by Weber[15] in developing a double-shell model to account for dips in some acoustic branches of the superconducting refractory carbides. Thus, the lattice-dynamical model consisted of conventional axially symmetric Born—von Kármán interactions between the ion cores plus *negative* short-range interactions between the charge- and mass-less shells which were coupled weakly to the ion cores. The dynamical matrix is given by the following expression:

$$\underline{\mathbf{D}}(\mathbf{q})=\underline{\mathbf{D}}_0(\mathbf{q})+\underline{\mathbf{K}}[\underline{\mathbf{K}}+\underline{\mathbf{R}}(\mathbf{q})]^{-1}\underline{\mathbf{R}}(\mathbf{q})\,, \tag{1}$$

where $\underline{\mathbf{D}}_0(\mathbf{q})$, $\underline{\mathbf{R}}(\mathbf{q})$, and $\underline{\mathbf{K}}$ represent the Born—von Kármán, the shell-shell, and the shell-core interactions, respectively.

The lowest, doubly-degenerate, optic, Γ-point frequency, Γ_2^+, is associated with modes where the two tellurium planes of the sandwich move with opposite phase in either the x or y direction and the palladium atoms are at rest. The frequency of the corresponding vibration of the tellurium atoms perpendicular to the planes, Γ_1^+, at about 4 THz is almost a factor of 2 higher. From this large ratio it is apparent that an essentially transverse interaction between nearest-neighbor tellurium atoms must be responsible for the low Γ_2^+ frequency. This has been incorporated in the model by including a transverse intershell force constant for the interactions between Te-Te nearest neighbors. This force constant had to be negative in order to produce a dip in the dispersion curves.

The dispersion curves obtained with this model by a least-squares fit to the majority of the experimental data are shown compared directly with the data in Fig. 3. We

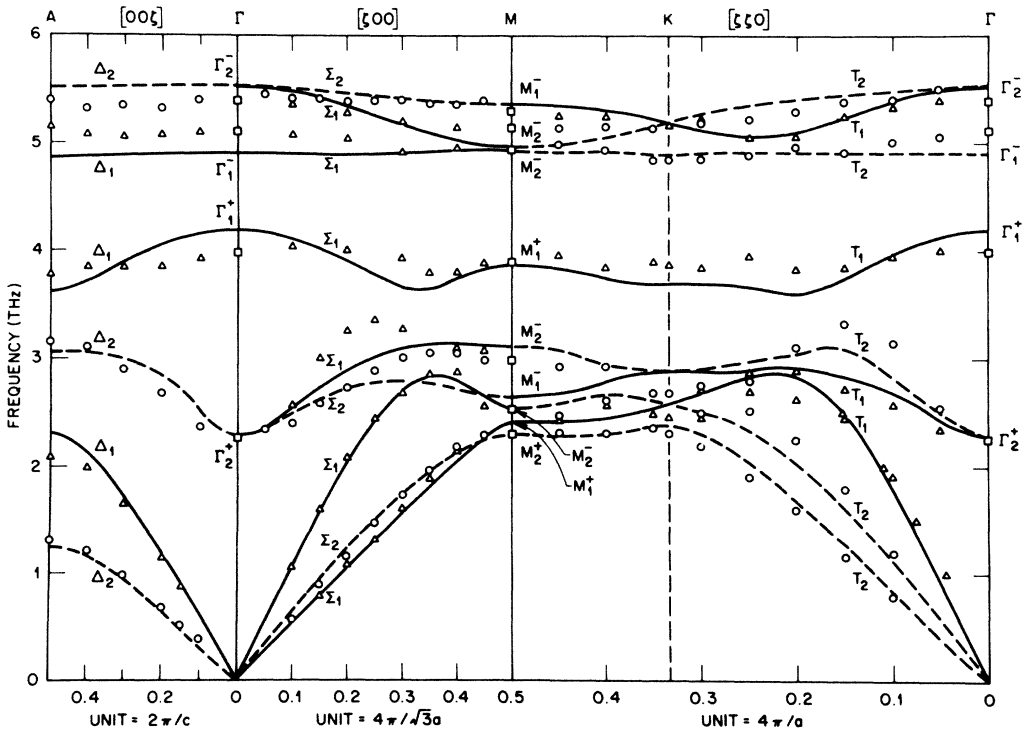

FIG. 3. Dispersion curves computed for the lattice-dynamical model consisting of axially symmetric Born—von Karman interactions to seventh-nearest neighbors together with shell interactions for tellurium atoms compared with the experimental data.

TABLE II. Force constants for model of lattice dynamics of $PdTe_2$.

Shell number	Radius (unit: a)	Nature of interaction	Force constants (dyn/cm) Born–von Kármán $F=\frac{\partial^2 V}{\partial r^2}$	$G=\frac{1}{r}\frac{\partial V}{\partial r}$	Shell-shell, shell-core
1	0.657 07	Pd-Te intrasandwich	41 480	10 176	
2	0.852 61	Te-Te intrasandwich	19 615	−3958	−730, 7697
3	0.863 88	Te-Te intersandwich	13 122	−31.8	−730, 7697
4	1.0	Te-Te basal plane	5910	−4978	
5	1.0	Pd-Pd basal plane	−221	4757	
6	1.117 08	Pd-Te intersandwich	2528	272	
7	1.196 35	Pd-Te intrasandwich	4668	240	

used 14 Born–von Kármán force constants for interactions up to seventh-nearest neighbor and two additional parameters for the shell interaction. The parameters for the fit are listed in Table II. The number of force constants is somewhat arbitrary. On the one hand we endeavored to limit the number of parameters since the application of axially symmetric forces is certainly too simplified for an anistropic crystal. At the same time we wanted to obtain a reasonably good description of the dispersion curves in order to make use of the model in identifying the experimental phonon groups in those regions where there are densely spaced and mutually interacting phonon branches.

From the structure of $PdTe_2$ it can be seen that the sandwich thickness is nearly identical to the intersandwich distance. The force constants for interactions between both intrasandwich and intersandwich Te-Te nearest neighbors can be compared from Table II. Although their values differ, this difference is of little consequence to the nature of the dispersion curves, since practically the same fit was obtained on making these two interactions identical. This is also true of the shell-shell interactions for which we could only determine the sum of the two force constants. For this reason we put them equal.

V. DISCUSSION

The quality of the fit obtained is reasonably good considering the simplicity of the model and the complexity of the experimentally determined dispersion curves. The significance of the shell interactions in modeling the strongly dispersive, low-energy, optic vibrations can be demostrated by calculating the dispersion curves using the same model parameters except that the shell interactions are turned off. This result is shown by the dotted lines in Fig. 4. Clearly, the influence of these shell interactions is restricted primarily to the lowest-energy optic branches around the Γ point.

From a comparison of intensities, measured at various reciprocal-lattice points, with those calculated using the best fit to the model, the Γ-point frequencies of the Γ_1^+ and Γ_1^- modes have been uniquely determined. This does not apply to the order of the Γ_2 modes because both contribute to the scattering cross section simultaneously. Our model attributes the higher of the two measured frequencies to the Γ_2^- mode. However, based on the experimental information only, the order of the two frequencies could also be reversed. Therefore, one fit was tried where the Γ_2^+ mode was forced to be the highest frequency (and the Γ_2^- the lowest). This fit resulted in completely unrealistic force constants and imaginary frequencies at several regions in the Brillouin zone. Thus, we believe that the model given in Table II is qualitatively correct although certainly too simplified to give a precise quantitative description of the dispersion curves for $PdTe_2$.

The use of axially symmetric forces must be considered only as an approximation. Furthermore, the shell interactions introduced in order to simulate electronic screening effects, are represented by only one force constant. This produces too sharp a drop in the lowest optic branch of the $[00\zeta]$ direction whereas for directions within the basal plane the structures in the calculated branches are less pronounced than those found experimentally. Likewise, the optic branch around 4 THz is much flatter than indicated by the model. We conclude that the phonon fre-

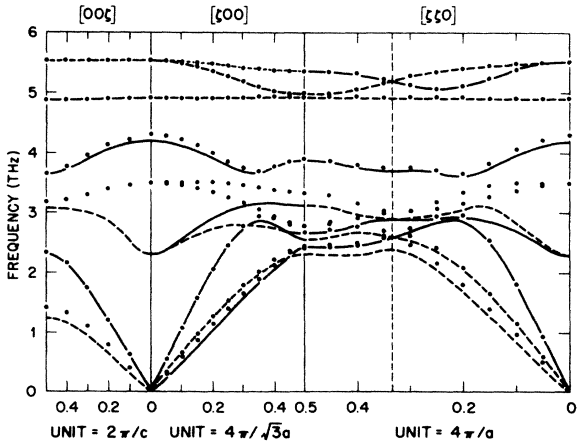

FIG. 4. Dotted curves illustrate the effect of turning off the shell interactions in the lattice-dynamical model for $PdTe_2$. Solid and dashed curves are reproduced from Fig. 3 for direct comparison.

quencies near Γ_1^+ are renormalized to some extent by the same mechanism which produces the dips in the lowest optic branches near Γ_2^+.

We have attempted to describe this behavior by a second model (M2) where we included longitudinal shell-shell interactions. In this calculation the shell-core force constant was the same as that in Table II (model M1) whereas the single transverse shell interaction was replaced by a longitudinal and a transverse force constant in such a manner that the Γ_2^+ frequency remained essentially unchanged. The Born—von Kármán force constants were redetermined by a least-squares-fit calculation. While with M2 we could achieve the aim of a better fit to the optic branches starting from Γ_1^+, adverse effects on other sections of the dispersion curves have lead to our favoring M1 in order to estimate some physical properties.

Using M1 we have calculated the phonon density of states, shown in Fig. 5, and the amplitude-weighted partial densities of states[16] of the Pd and Te atoms from which the Debye cutoff frequencies ν_n ($n \neq 0$, $n > -3$) have been calculated in the usual manner. These frequencies are given in Table III from which it can be seen that for $-1 \leq n \leq 2$, $(M\nu_n^2)_{\mathrm{Pd}} \approx 2(M\nu_n^2)_{\mathrm{Te}}$, where M is the atomic mass. This observation will be of some consequence for T_c, as, owing to the dominant p character of the electronic density of states at the Fermi energy,[11] the Te atoms yield the major contribution to the electron-phonon coupling constant. Also, from the phonon density of states we have calculated the lattice heat capacity which is in good agreement with the measured data.[17] ν_{-3} corresponds to a Debye temperature of 216 K.

Jan and Skriver[11] have performed the most recent band-structure calculations for $PdTe_2$. According to their calculations the unhybridized bands near the Fermi energy are Pd 5s and Te 5p. The Pd 4d bands form a very narrow band about 2 eV below the Fermi energy. In their full band-structure calculation, however, the Pd 5s band is pushed to higher energies while the middle energy range contains strongly hybridized (Te 5p)—(Pd 4d) bands. Therefore we may assume that the electronic density of states near the Fermi energy is mainly of p character with admixtures of d character.

The Fermi surface consists of three sheets: a closed hole sheet at Γ, a small electron pocket at K, and a rather complex electron sheet at K with thin hoses interconnecting different K points in the Z direction. It may be the scattering of electrons across these hoses which causes the

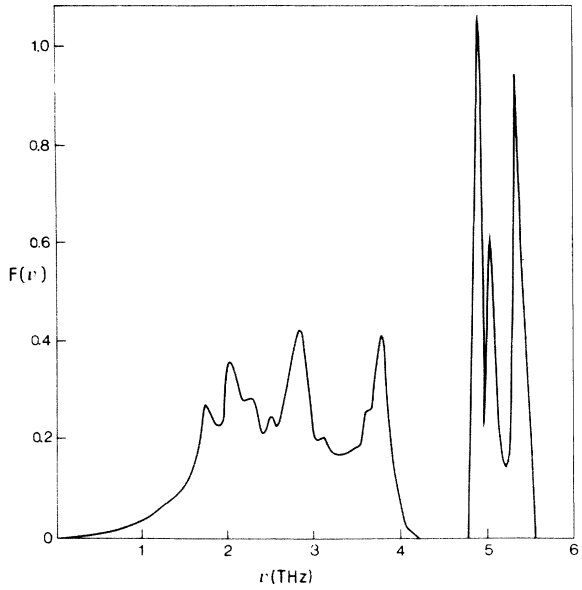

FIG. 5. Phonon density of states for $PdTe_2$, calculated from the model given in Table II.

dip in the lowest energy optical branches close to the Γ point. From Fig. 4 of the paper by Jan and Skriver one can estimate the diameter of the hoses to be of the order of $0.15AH$ ($=0.05 \times 4\pi/a$) which roughly corresponds to the half-width of the dip observed in the low-energy LO [$\zeta\zeta 0$] branch.

Another explanation[18] for the low Γ_2^+ frequency in $PdTe_2$ results from the fact that the electron bands forming the two electron Fermi surfaces penetrate only slightly below the Fermi energy with minimum energies, $E - E_F$, at the K point of about 300 meV. Except for a vary small spin-orbit splitting they are degenerate along KH. A distortion of the lattice by a phonon will lift these degeneracies and eventually push one band completely above the Fermi level while the energy of the other is reduced resulting in a lowering of the total energy associated with this phonon mode. A similar effect has been suggested to be responsible for the anomalous depression of the [00ζ] LO-phonon frequency in Ti near the Γ point.[19] Although we are not able to substantiate this hypothesis by explicit calculations, such an effect would be most pronounced for the Γ_2^+ mode which produces the largest distortion of the

TABLE III. Debye cutoff frequencies (in THz) for the various moments of the density of states of $PdTe_2$ and of the amplitude-weighted partial densities of states of the two constituents calculated from the model outlined in Sec. IV. The last row demonstrates the relatively soft Te spectrum.

n	−3	−2	−1	0	1	2	3
$PdTe_2$	4.48	4.26	4.30	4.46	4.65	4.82	4.97
Pd		5.44	5.88	6.07	6.16	6.16	6.12
Te		3.91	3.80	3.82	3.89	3.99	4.10
$\frac{(M\nu_n^2)_{\mathrm{Te}}}{(M\nu_n^2)_{\mathrm{Pd}}}$		0.618	0.500	0.469	0.477	0.504	0.538

Te sublattices.

As a consequence, an anomalous temperature dependence of the Γ_2^+ frequency should be expected because the renormalization of the phonon frequency is reduced when the unoccupied band above the Fermi energy becomes populated by thermal excitations. Our measurements did not show such an effect when cooling from room temperature to 10 K. However, as the splitting required to empty the upper electronic band has to be in the range of a few hundred meV, much higher temperature changes than those applied in our experiments will be required in order to provide a decisive test for the above explanation.

It is of interest to compare our results with those available for isostructural compounds. Most of the available data[9,14,20,21] are for the acoustic branches where one point of concern has been the appearance of a slight q^2 dependence at low q in the dispersion curves for transverse modes propagating in the basal plane but polarized perpendicular to it, arising from weak intersandwich forces. For $SnTe_2$ ($c/a=1.615$),[14] $NiTe_2$ (1.368),[20] and $PdTe_2$ (1.270) the degree of curvature is almost negligible by comparison with $TiSe_2$ (1.698),[9] indicating that these compounds are not significantly two dimensional in character at the microscopic level, despite the ease with which they can be cleaved.

As some optic branches have been measured for $TiSe_2$ (Ref. 9) a further comparison with this compound has been attempted. For this aim we have plotted in Figs. 6(a) and 6(b) the Σ_2 branches of the two compounds. There are rather striking differences between these two data sets. The two Γ_2 frequencies, which are the highest and lowest optic Γ-point frequencies in $PdTe_2$, are almost degenerate in $TiSe_2$. The lower optic branch in $TiSe_2$ shows an anticrossing with the acoustic branch and a rather low M-point frequency, which is a consequence of the soft L-point mode associated with the CDW transition. These features are absent in $PdTe_2$.

When tracing the origin of these discrepancies we have to consider that the atomic masses and the atomic packing are different in the two compounds. In $TiSe_2$, which has a c/a ratio of 1.69, the Se atoms form a nearly close-packed hexagonal arrangement. Thus, the three smallest Se-Se distances are almost equal, whereas in $PdTe_2$ the corresponding Te-Te distances differ by as much as 16%. We have investigated the influence of the atomic masses and the interatomic distances on the phonon branches with a model calculation, in which we used the atomic masses of $TiSe_2$ and the force constants of $PdTe_2$. In an attempt to account for the interatomic distances in $TiSe_2$ the latter were modified according to

$$f_2=f_1\left[\frac{R_1}{R_2}\right]^3\frac{v_2}{v_1}\,. \tag{2}$$

In this relation f stands for the longitudinal or the transverse force constants, R is the interatomic distance associated with a particular force constant, and v is the volume of the unit cell. The labels 1 and 2 refer to $PdTe_2$ and $TiSe_2$, respectively. As we believe that the dips in some optic branches, which are accounted for in our model by the shell interactions, are a unique feature of $PdTe_2$, we have omitted the shell interactions in this calculation.

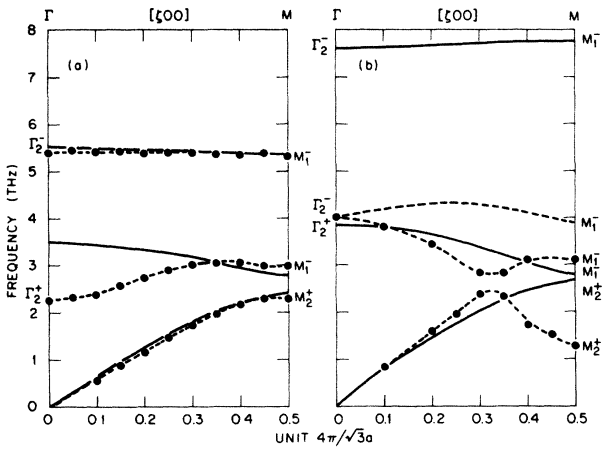

FIG. 6. Σ_2 phonon branches for (a) $PdTe_2$ and (b) $1T$-$TiSe_2$. The dashed lines are a guide to the eye through the experimental points which for $TiSe_2$ are taken from Ref. 9 with the highest Σ_2 branch being a model calculation by these authors. The solid lines have been calculated as described in Sec. V.

The results for the Σ_2 branches are shown by the solid lines in Fig. 6(b). The comparison with the model calculation for $PdTe_2$ (without shell interaction) reproduced on Fig. 6(a), shows that these mass and distance corrections have enlarged the difference between the Γ_2^- and Γ_2^+ frequencies, contrary to the experimental observations. Qualitatively, such analysis demonstrates that the considerable differences in the phonon dispersion curves of these two compounds cannot be accounted for by differences in the atomic masses and the atomic packing. Quantitatively, however, Eq. (2) can only represent a crude description of the dependence of the force constants on distance. For example, it takes no account of the possible influences of the electronic band structure.

Within the framework of our lattice-dynamical model the only way to bring the Γ_2^- frequency down to the Γ_2^+ frequency is by reducing drastically the first-nearest-neighbor Ti-Se force constants. This is in accordance with the analysis of Wakabayashi *et al.*[9] who showed that the CDW transition in $TiSe_2$ may be attributed mainly to an instability of the Ti—Se bond.

Finally, although there is hitherto no evidence for the formation of a CDW in $PdTe_2$ at low temperatures, it could not be ruled out that some type of modulated structure may already exist at room temperature, as in $1T$-$TaSe_2$.[22] Therefore a search was made at room temperature for crystallographic evidence of a CDW, but without success. This was accomplished by selective neutron diffraction scans, x-ray precession photographs, and electron diffraction.

VI. CONCLUSIONS

The lattice dynamics for $PdTe_2$ can be modeled reasonably well using axially symmetric Born—von Kármán interactions out to seventh-nearest neighbors together with shell-model contributions for the intersandwich and in-

trasandwich Te-Te nearest neighbors. The latter primarily influence the shapes of the low-energy optic branches for which a dip in the vicinity of the Γ point was observed. Further experimental and theoretical work is needed before a microscopic origin for this feature of the dispersion curves can be undersood and the occurrence of superconductivity in this compound adequately explained.

ACKNOWLEDGMENTS

The $PdTe_2$ crystal on which the dispersion curves were measured was grown by A. Vas (Monash University) for whom financial support from the Australian Research Grants Scheme is acknowledged. Two of us (T.R.F. and W. R.) are most grateful to the Oak Ridge National Laboratory for the opportunities to spend extended periods in Oak Ridge and to the staff of the Solid State Division for their kind hospitality. We are indebted to B. N. Harmon for pointing out a possible explanation for the dips in the low-energy optic branches. We wish to thank B. S. Borie for the x-ray precession photographs, J. Narayan for the electron diffraction observations, and N. Wakabayashi for assistance and helpful discussions during the early stages of this investigation. This research was sponsored by the Division of Materials Sciences, U. S. Department of Energy, under Contract No. DE-AC05-840R21400 with Martin Marietta Energy Systems, Inc.

---

*Permanent address: Department of Physics, Monash University, Clayton, Victoria, Australia 3168.

†Permanent address: Kernforschungszentrum Karlsruhe GmbH, Institut für Nukleare Festkörperphysik, Postfach 3640, D-7500 Karlsruhe, Federal Republic of Germany.

[1]J. A. Wilson and A. D. Yoffe, Adv. Phys. **18**, 193 (1969).

[2]B. W. Roberts, J. Phys. Chem. Ref. Data **5**, 581 (1976); and U. S. National Bureau of Standards Technical Note No. 983 (1978) (unpublished).

[3]T. F. Smith, R. N. Shelton, and R. E. Schwall, J. Phys. F **5**, 1713 (1975).

[4]G. K. Bristow, C. A. Cornelius, T. F. Smith, and T. R. Finlayson, J. Phys. F **8**, 2165 (1978).

[5]C. W. Chu, V. Diatsohenko, C. V. Huang, and F. J. DiSalvo, Phys. Rev. B **15**, 1340 (1977).

[6]D. E. Moncton, J. D. Axe, and F. J. DiSalvo, Phys. Rev. B **16**, 801 (1977).

[7]K. C. Woo, F. C. Brown, W. L. McMillan, R. J. Miller, M. J. Schaffmann, and M. P. Sears, Phys. Rev. B **14**, 3242 (1976).

[8]F. J. DiSalvo, D. E. Moncton, and J. V. Waszczak, Phys. Rev. B **14**, 4321 (1976).

[9]N. Wakabayashi, H. G. Smith, K. C. Woo, and F. C. Brown, Solid State Commun. **28**, 923 (1978).

[10]M. J. Clark, thesis, Monash University, 1979.

[11]H. W. Myron, Solid State Commun. **15**, 395 (1974); J.-P. Jan and H. L. Skriver, J. Phys. F **7**, 1719 (1977).

[12]P. J. Orders, J. Liesegang, R. C. G. Leckey, J. G. Jenkin, and J. D. Riley, J. Phys. F **12**, 2737 (1982).

[13]A. Lyons, D. Schleich, and A. Wold, Mat. Res. Bull. **11**, 1155 (1976).

[14]J. L. Brebner, S. Jandl, and B. M. Powell, Nuovo Cimento B **38**, 263 (1977).

[15]W. Weber, Phys. Rev. **38**, 5082 (1973).

[16]B. P. Schweiss, B. Renker, E. Schneider, and W. Reichardt, p. 189 in *Superconductivity in d- and f-Band Metals,* edited by D. H. Douglass, (Plenum, New York, 1976).

[17]T. R. Finlayson, D. M. Kroeger, W. Reichardt, and J. O. Scarbrough (unpublished).

[18]B. N. Harmon (private communication).

[19]C. Stassis, D. Arch, B. N. Harmon, and N. Wakabayashi, Phys. Rev. B **19**, 181 (1979).

[20]M. Sato and K. Abe, J. Phys C **12**, L613 (1979).

[21]W. G. Stirling, B. Dorner, J. D. N. Weeke, and J. Revelli, Solid State Commun **18**, 931 (1976).

[22]J. A. Wilson, F. J. DiSalvo, and S. Mahajan, Phys. Rev. Lett. **32**, 882 (1974).